AIP | Journal of Applied Physics

Tuning the wavelength of lasing emission in organic semiconducting laser by the orientation of liquid crystalline conjugated polymer

Myoung Hoon Song, Bernard Wenger, and Richard H. Friend

Citation: Journal of Applied Physics **104**, 033107 (2008); doi: 10.1063/1.2959339
View online: http://dx.doi.org/10.1063/1.2959339
View Table of Contents: http://scitation.aip.org/content/aip/journal/jap/104/3?ver=pdfcov
Published by the AIP Publishing

Tuning the wavelength of lasing emission in organic semiconducting laser by the orientation of liquid crystalline conjugated polymer

Myoung Hoon Song, Bernard Wenger, and Richard H. Friend[a)]
Cavendish Laboratory, University of Cambridge, Cambridge CB3 0HE, United Kingdom

(Received 8 November 2007; accepted 26 May 2008; published online 6 August 2008)

We report the optical pumping of one-dimensional distributed feedback (DFB) conjugated polymer devices using a uniaxially aligned liquid crystalline polymer, poly(9,9-dioctylfluorene). We can independently select the alignment direction (via a rubbed polyimide layer) and the DFB structure (via nanoimprinting). In comparison with unaligned film, we show that lasing threshold is substantially reduced when absorption is parallel to the aligned direction ($\sim$20.0 μJ cm^{-2} pulse^{-1}). This is mainly due to the higher absorption coefficient estimated in the table by calculating the exciton densities at each threshold value. We also report the control of lasing wavelength through independent selection of alignment direction and DFB orientation, which is achieved through the control of the effective refractive index of waveguide (n_{eff}). © *2008 American Institute of Physics*. [DOI: 10.1063/1.2959339]

I. INTRODUCTION

Conjugated polymers are considered attractive as gain media for laser and broadband optical amplifiers[1,2] due to the high photoluminescence quantum efficiencies, broad gain range, tunability throughout the visible spectrum, and scope for simple fabrication processing. Continuing efforts have also been made to realize an electrically pumped organic laser by reducing laser threshold and increasing charge mobility. For an electrically pumped organic laser, high current densities are required within a thin polymer film that shows higher optical gain and lower thresholds of stimulated emission. Some reports have also demonstrated much lower thresholds of stimulated emission or amplified spontaneous emission (ASE) by aligning organic molecules.[3–6] In this respect, polyfluorenes, such as poly(9,9-dioctylfluorene) (F8) and poly(9,9-dioctylfluorene-co-benzothiadiazole) (F8BT), are very attractive materials due to high quantum efficiencies, high optical gain, and good electrical properties.

There are many reports of optically pumped conjugated polymer lasers in various structures, such as distributed feedback (DFB) (Refs. 7–10), microcavities,[11–13] photonic crystals,[14] and so on. Among them, the DFB structure has received much attention as it offers long gain lengths resulting in very low thresholds. It is thus a candidate for an organic semiconducting laser structure for continuous wave lasing and electrically pumped organic diode lasers, both of which have many practical applications, from medicine to telecommunication. Moreover, this DFB structure can be easily combined with electrical devices such as organic light emitting diodes and light emitting organic transistors.[15] It provides a way to tune the wavelength of the lasing emission through the control of the grating dimension (Λ) (Refs. 16–18) or the film thickness of active layer[8,9,19] that controls the effective index of the waveguide mode (n_{eff}) that can be changed. In this paper, we report a method of tuning the wavelength of lasing emission with a lowered threshold by aligning F8 molecules.

II. EXPERIMENT

The conjugated polyfluorene polymer F8 was used in these experiments. The F8 ($M_n \sim 92\,700$ and $T_g \sim 51$ °C) was dissolved in *p*-xylene solutions, and F8 films were fabricated by spin coating the solution onto glass substrates. The film thickness was controlled according to solution concentration and spin speed and was measured using a Sloan Dektak surface profilometer.

To align this thermotropic polymer, a polyimide (PI2525, HD Microsystems) alignment layer was coated on a glass substrate and then rubbed unidirectionally at room temperature. After polymer deposition on rubbed polyimide the F8 films were preannealed for 10 min at 110 °C below the melting point of F8 to try to induce crystallization prior to aligning. The films were then cured at 275 °C for 17 min in a glovebox to prevent oxidation at high temperature and quenched quickly to room temperature, and then well-aligned F8 films were obtained.

These F8 films were then patterned using a soft lithographic technique known as hot embossing.[20] A holographic grating (GH13–36U, 3600 lines/mm, THORLABS) was used as a master with a period (Λ) of 278 nm (12.7 × 12.7 mm). An ethylene(tetrafluoroethylene) (ETFE) replica (nonadhesive to polymer) was used and placed on the master.[21] Then this assembly was put into an Obducat nanoimprinter (Obducat AB, Sweden), then imprinted at 220 °C (above T_g) and 20 bars for 5 min, and then cooled down to 70 °C (below T_g). Subsequently, the patterned ETFE replica was placed against the F8 film and imprinted at 90 °C (above T_g) and 20 bars for 5 min, and then cooled down below T_g before releasing the pressure. This procedure gave a one-dimensional (1D) patterned F8 film with a period (Λ) of 278 nm and a depth of 40 nm.

[a)]Electronic mail: rhf10@cam.ac.uk.

The orientation of polymer chain was also examined using a crossed-polarizers microscope (Olympus BX60). The degree of the polymer chain orientation was examined using polarized UV-vis absorption measurements at wavelengths corresponding to the polymer absorption peak (~396 nm). The aligned F8 film was placed in a HP8453 UV-vis spectrometer (Hewlett–Packard), and the linear polarizer was placed in front of the F8 film for different polarized light incidences.

For ASE and lasing measurements, a 355 nm pulsed laser beam with a third harmonic light from a Nd:YVO4 (yttrium orthovanadate) *Q*-switched diode laser (AOT-YVO-250QSPX: Advanced Optical Technology, Ltd.) was used as an optical pumping source. The pulse width was 500 ps, and the repetition rate was 1 kHz. The pumping laser beam was focused on the sample surface at oblique incidence (about 35°), and the emission from the sample was collected in a fiber-coupled spectrograph (USB 4000: Ocean Optics, Inc.), which was normal to the substrate.

III. RESULT AND DISCUSSION

We first examined the degree of alignment using polarized absorption and optical microscopy. Figure 1(a) shows the textures of the aligned F8 film examined using crossed-polarizers microscope. The micrographs in Fig. 1(a) correspond to textures measured at rotational angles of ϕ=0°, +45°, −45°, and 135°, where the rotation angle is between the polarization direction of one polarizer and rubbing direction. Most of the domains look bright at ±45° and 135°, whereas they appear dark at 0°. Thus, we can confirm that homogeneous alignment of F8 films is achieved. Figure 1(b) shows the polarized UV-vis absorption spectra of the aligned F8 layer at 0° (red line) and 90° (black line) polarized incident angles at the chain orientation. Maximum absorption is along the polymer chain orientation director in the aligned F8 sample, i.e., when the polarization of incident light is parallel to the orientation of polymer chain. Minimum absorption is the case when the polarization of incident light is perpendicular to the orientation of polymer chain. The dichroic ratio at the maximum of the absorption band (396 nm) is 11.4, and the polar light absorption plot obtained upon polarization rotation is shown as inset in Fig. 1(b).

We note that under our conditions, the uniaxial alignment direction was not affected by the subsequent nanoimprinting. However, Zheng *et al.*[20] demonstrated the uniaxial alignment of F8BT (M_n~9 000) by means of nanoconfinement during hot embossing. In this experiment, the orientation of F8 molecules did not change after hot embossing by polarized absorption measurement. The absence of alignment may be due to higher molecular weight of F8 molecules (M_n~92 700) used in this experiment and shorter periodicities of the nanostructures.

Figure 2(a) shows the DFB laser structure. This DFB laser device consists of a corrugated F8 polymer film on top of uniaxially rubbed polyimide film and substrate. For a corrugated DFB laser structure, laser emission occurs at the Bragg wavelength λ,

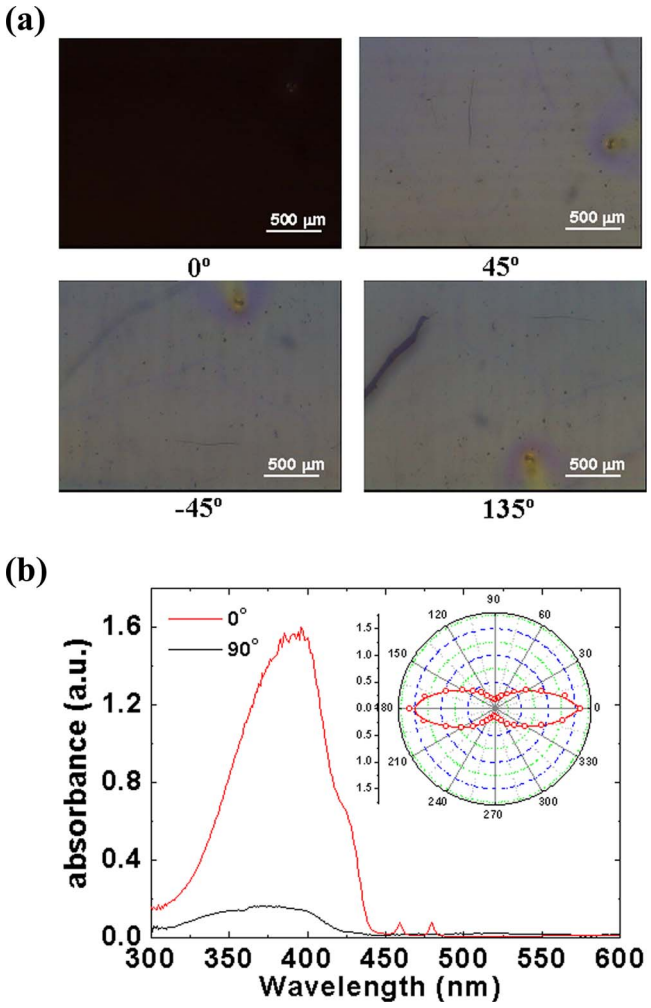

FIG. 1. (Color online) (a) Crossed-polarizers micrographs of the aligned F8 film with the polyimide alignment film (upper left ϕ=0°, upper right ϕ=45°, lower left ϕ=−45°, and lower right ϕ=135°). (b) Polarized UV-vis absorption spectra of the aligned F8 layer at 0° (red line) and 90° (black line) polarized incident angles at the chain orientation. The inset shows polar plot of angular dependence of polarized UV-vis absorption spectra of the aligned F8 layer.

$$m\lambda = 2n_{\text{eff}}\Lambda, \tag{1}$$

where λ is the vacuum wavelength of light, Λ is the period of grating, and n_{eff} is the so-called effective refractive index of the waveguide. For m=2 (second order), the lasers are surface emitting.

Figure 2(b) shows a series of measured emission spectra from 1D anisotropic F8 laser samples with different F8 film thicknesses. For comparison, a series of measured lasing emission spectra from 1D isotropic F8 laser sample cell is also shown in Fig. 2(c). The two important observations from the data in Figs. 2(b) and 2(c) are as follows: (1) Two lasing spectra at the same wavelength (458 nm) were observed at 62-nm-thick aligned F8 film and 147-nm-thick unaligned F8 film, and (2) the tuning range was 445–469 nm. The reason in (1) is the higher refractive index value in the light propagation direction obtained by aligning the F8 layer.

Figure 2(d) shows selected spectra of angle-resolved polarized emission featuring sharp peaks from scattered TE waveguide modes in 193-nm-thick anisotropic F8 laser

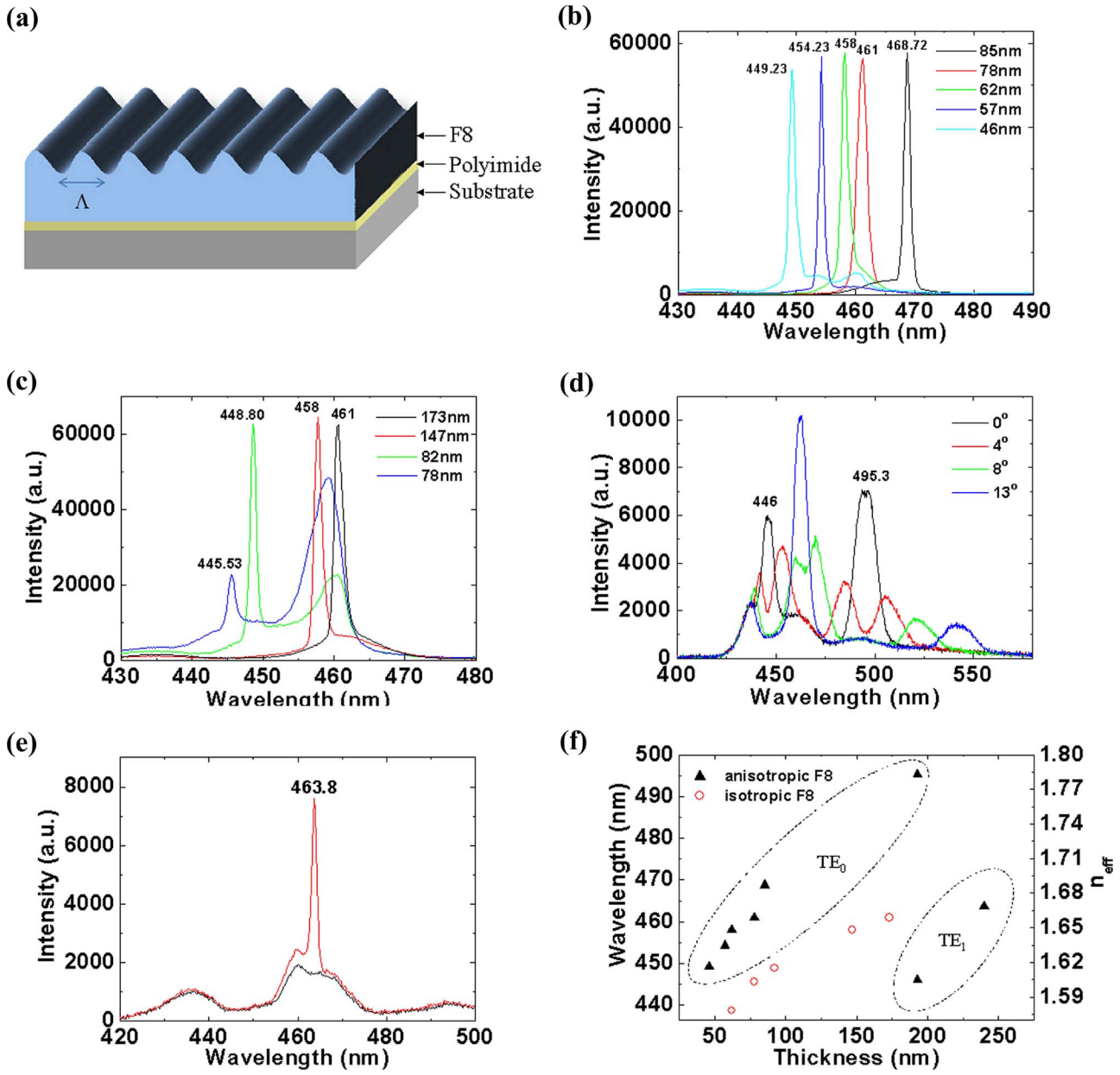

FIG. 2. (Color online) (a) Schematic illustration of polymer DFB laser with corrugation of 278 nm period and a depth of 40 nm. Lasing spectra measured (b) for the anisotropic F8 laser sample cell and (c) for the isotropic F8 laser sample cell with various film thicknesses of F8 layer. (d) The few photoluminescence spectra of TE-polarized waveguide. The graph shows the effective index vs the wavelength for TE_0 and TE_1 waveguide modes in the 193-nm-thick aligned F8 film. (e) TE_1-polarized lasing spectra from the anisotropic F8 laser cell (the polarization beam is parallel to the F8 chain alignment) with 240 nm thickness. (f) The lasing wavelengths and effective refractive index of the anisotropic F8 laser sample cell (black-filled triangles) and the isotropic F8 laser sample cell (red open circles) as a function of F8 film thickness.

sample. Two 446 and 495.3 nm emission peaks (black) instead of a lasing emission were shown at $m\lambda = 2n_{\text{eff}}\Lambda$. The peak wavelength splitting at a given angle was observed because the grating scatters waveguided light traveling in opposite directions. As the thickness of the anisotropic F8 layer was increased further (240 nm), TE_1 mode lasing was observed at 463.8 nm, as shown in Fig. 2(e).

After measuring the lasing emission spectra, the effective refractive index of each spectrum could be calculated by inserting the peak wavelengths at 0° in Eq. (2),[22]

$$n_{\text{eff}} = \frac{\lambda}{\Lambda} \pm \sin(\theta). \tag{2}$$

The wavelengths of lasing modes and n_{eff} for TE_0 and TE_1 waveguide modes in the F8 film are plotted versus the thickness of the active layer in Fig. 2(f). We note first that the lasing wavelength and n_{eff} of anisotropic and isotropic F8 laser samples are different from the same thickness of F8 films. Second, the TE_0 mode shifts toward longer wavelengths due to the increase in effective refractive index as the thickness is increased. Finally, another mode (TE_1) appears at shorter wavelengths and is shifted toward the longer wavelengths repeatedly in the anisotropic F8 laser sample.

For the comparison of threshold and gain between the anisotropic and isotropic F8 sample cells, four different experimental configurations were used, as shown in Fig. 3(a).

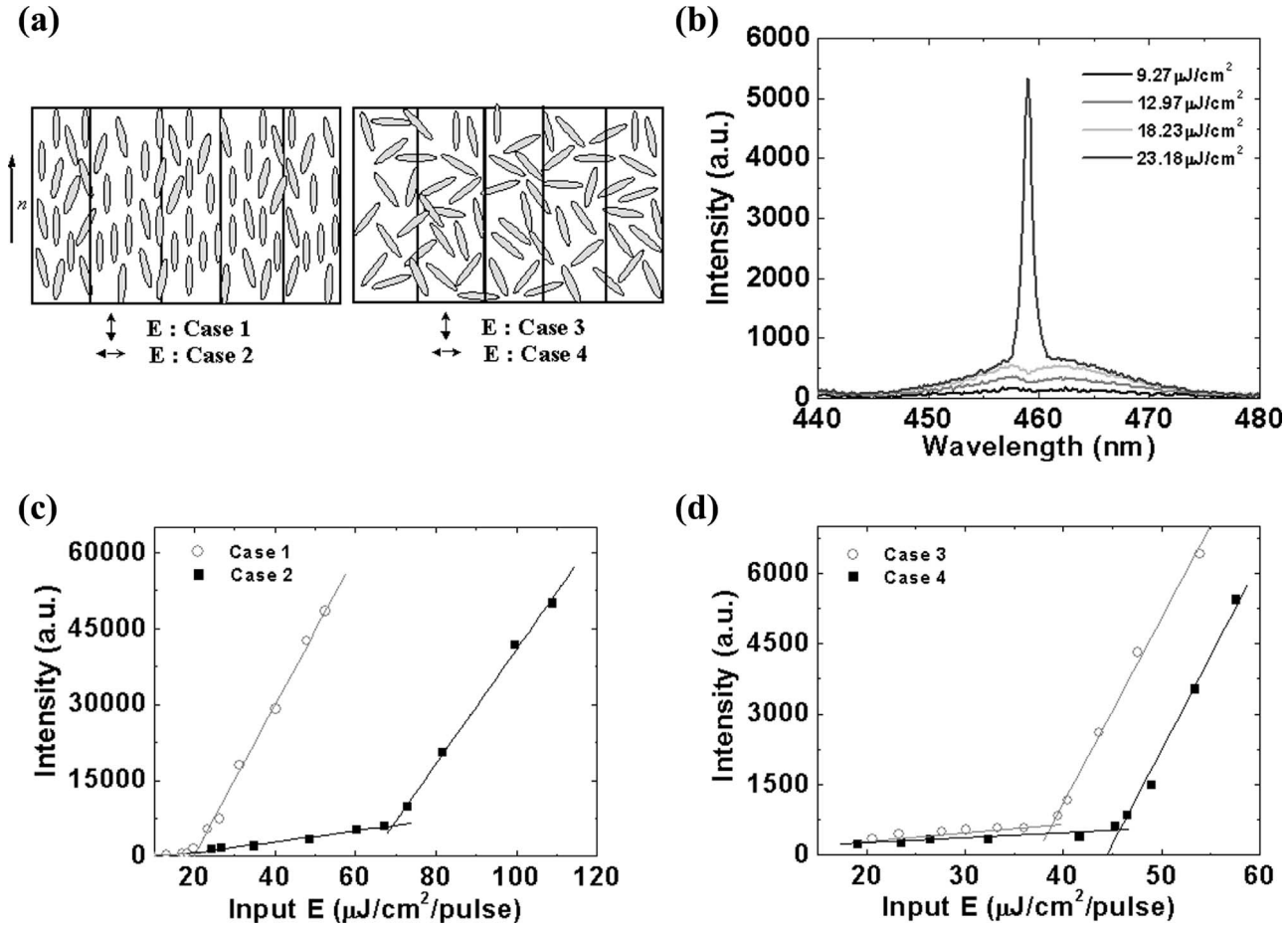

FIG. 3. (a) Schematic illustration of four different excitation configurations. The black lines correspond to grating lines, and the rod shapes correspond to F8 molecules. (b) TE-polarized emission spectra from the anisotropic F8 laser cell (the polarization beam is parallel to the F8 chain alignment) with 62 nm thickness for pump energies above and below the threshold of 20 $\mu J/cm^2$ pulse. (c) Threshold behavior in the anisotropic F8 laser cell. The polarization beam parallel (perpendicular) to the F8 chain alignment corresponds to case (1) [case (2)]. (d) Threshold behavior in the isotropic F8 laser cell. The polarization beam parallel (perpendicular) to the F8 chain alignment corresponds to case (3) [case (4)].

These configurations look very similar to Refs. 3 and 4 in ASE experiments. In case (1), the incident excitation beam was polarized parallel to the chain alignment axis and grating lines, maximizing the absorption in the anisotropic F8 sample cell. The emitted light of the TE waveguide mode parallel to the alignment direction propagates along one axis by grating within the film plane; thus a higher waveguide confinement of TE mode can be expected due to the higher refractive index in this direction. In case (2), the incident excitation beam is polarized perpendicular to the chain alignment axis and grating line, minimizing the absorption in the anisotropic F8 sample cell. However, the higher waveguide confinement of TE mode is the same as in case (1). In both cases (1) and (2), it is favorable for amplification as the transition dipole moments lie nearly parallel to the polymer chains and light is diffracted in the direction perpendicular to the grating lines. Excitation conditions for (3) and (4) were the same for (1) and (2), respectively, but the F8 films were unaligned. It was difficult to compare the thresholds among the four cases because both the amount of light absorbed and the effective indices changed. In order to compare the devices, we adjusted the thickness of the active polymer films to match the same emission wavelength—in other words, the same effective refractive index. The film thickness of cases (1) and (2) is 62 nm, and the film thickness of cases (3) and (4) is 147 nm. Figure 3(b) shows the emission spectra of case (1) measured normally to the waveguide surface when pumped both below and above (black line, 23.2 $\mu J/cm^2$ pulse) lasing threshold. The Bragg dip was visible below the threshold, and the lasing mode appeared close to the dip wavelength (458 nm). The laser linewidth was measured to be ~1 nm, limited by the resolution of our spectrometer.

Figures 3(c) and 3(d) show the light input-output characteristics of cases (1)–(4). In a 62-nm-thick anisotropic F8 laser sample, the threshold of case (1) (~20.0 $\mu J/cm^2$ pulse) was lower than that of case (2) (~69.0 $\mu J/cm^2$ pulse)—as expected due to the strong light absorption when the excitation beam was polarized parallel to the orientation of F8 molecules. Whereas the thresholds of cases (3) and (4) did not show large different threshold values (39.2 and 45.7 $\mu J/cm^2$ pulse, respectively) even if a little difference in these cases might be due to the effect of incident pump polarization.[23] To explore further the difference between the anisotropic and isotropic F8 lasers, the relationship between the net gain coefficient g, the confinement factor Γ, and the material gain coefficient g_{mat} should be considered.[24]

TABLE I. Exciton densities and threshold values for lasing in different excitation conditions.

	Threshold (μJ/cm^2)	Photon flux (photon/cm^2)	OD	T (%)	Exciton density at threshold (exciton/cm^2)	Film thickness (nm)	Exciton density at threshold (exciton/cm^3)
Aligned F8 (Parallel)	20	3.57×10^{13}	0.76	17.38	2.9×10^{13}	62	4.7×10^{18}
Aligned F8 (Perpendicular)	69	12.32×10^{13}	0.136	73.11	3.3×10^{13}	62	5.3×10^{18}
Unaligned F8 (Parallel)	38.8	6.93×10^{13}	1.02936	9.35	6.3×10^{13}	147	4.3×10^{18}
Unaligned F8 (Perpendicular)	45.7	8.16×10^{13}	1.02936	9.35	7.4×10^{13}	147	5.0×10^{18}

$$g = \Gamma g_{\mathrm{mat}} \quad \text{(if waveguide loss is neglecting)}. \tag{3}$$

For a given thickness, Γ is higher in anisotropic films because the higher index value in anisotropic films has a significant effect on the waveguiding and confinement. However, we found that the confinement of the isotropic F8 film ($\sim$0.75) in this study was better than that of the anisotropic F8 film ($\sim$0.51) due to the larger thickness of the isotropic F8 layer, whereas the outcoupling should be higher in the aligned film.[25]

Next, g_{mat} was also considered between the anisotropic and the isotropic layers. In general, g_{mat} can be expressed by $g_{\mathrm{mat}}=\sigma_{\mathrm{em}}N_{\mathrm{ex}}$, where N_{ex} is the exciton density and σ_{em} is the stimulated emission cross section.[26,27] Exciton densities at each threshold value were estimated, as shown in Table I. Exciton densities at each threshold value were similar even when the thickness of the anisotropic F8 layer (62 nm) was much thinner than that of the isotropic F8 layer (147 nm). This arises because the anisotropic F8 film absorbs more incident excitations than the isotropic F8 film, and it has enough excitons to start the lasing action. As for σ_{em}, it depends on the alignment of the molecular transition dipole moments with the polarization of stimulated emission (TE mode), i.e., anisotropic F8 layer has a higher absorption coefficient and increase in the stimulated emission cross sec-

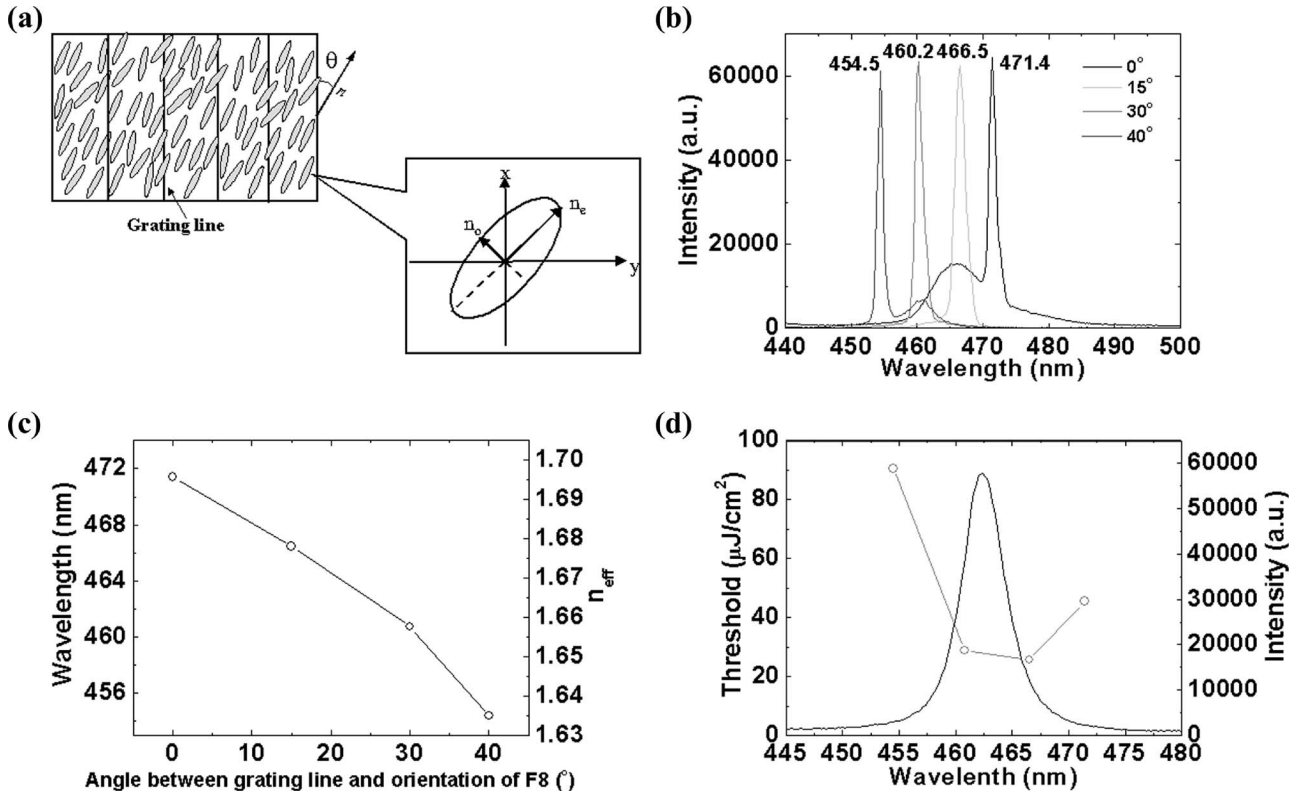

FIG. 4. (a) Schematic illustration of tunable DFB F8 laser sample cell. The arrow corresponds to the director of F8 molecules, and the angle is between the grating line and the orientation of F8. (b) Lasing spectra measured for the anisotropic F8 laser sample cell with different angles between the grating line and the orientation of F8. (c) Lasing wavelengths and effective refractive index of the anisotropic F8 laser sample cell (black open circles) as a function of angles between the grating line and the orientation of F8. (d) Threshold energy as a function of laser wavelength for the anisotropic F8 laser sample cell with different angles between the grating line and the orientation of F8. The ASE (black solid line) is shown for gain region.

tion (σ_{em}), as predicted by Einstein coefficients[2] or McCumber[28] relation. After all, the anisotropic F8 layer has higher gain (g_{mat}).

As discussed before, the confinement was better in the thick isotropic F8 film, and the exciton densities at each threshold value were almost the same. It means higher σ_{em} in anisotropic F8 layer may be an important parameter in counterbalancing confinement effect and showing lower threshold in anisotropic F8 DFB laser sample.

Generally, the emission wavelength of DFB lasers can be tuned by the control of the grating dimension (Λ) or the film thickness of the active layer. Here, we show another way of tuning the wavelength of DFB lasers. Figure 4(a) shows the schematic illustration of the tunable DFB laser structure, together with the aligned F8 polymer molecules. The effective refractive index of the TE lasing waveguide mode can be tuned by the orientation of F8 molecules, i.e., by the control of the angle between the alignment direction of F8 and the grating lines. The tunable wavelength of lasing emission can be achieved through the control of the direction of the aligned F8. Figure 4(b) shows a series of lasing emission spectra from the 1D DFB laser with the anisotropic F8 films as a function of angles between the alignment direction of the aligned F8 and grating orientation. Here, the wavelength of lasing emission was set at the edge of the gain spectrum (~470 nm) by the adjustment of the anisotropic F8 film thickness (88 nm), and the wavelength of lasing emission shifted toward the shorter wavelength as the angle was increased. The lasing wavelength and n_{eff} are plotted versus the angle between the alignment direction of the aligned F8 and DFB orientation in Fig. 4(c). The wavelength shift of lasing peaks was about 17 nm by controlling angle and this shift of lasing wavelength originated from the decrease in n_{eff} in the anisotropic F8 films by the inducing angle. Figure 4(d) shows the threshold of 1D DFB laser with the anisotropic F8 active layer as a function of wavelength. In general, the lowest threshold can be obtained at ASE maximum where the material gain is the highest and the shape of the threshold curve looks like the inverse of ASE peak.

In conclusion, we presented a study of the 1D DFB conjugated polymer device using a uniaxially aligned liquid crystalline F8 and compared the differences between the anisotropic and isotropic F8 laser devices. It demonstrates the following characteristics: (1) the different wavelengths of lasing emission at the same thickness due to the change in refractive index of F8 active layer after aligning; (2) the achievement of remarkable lowering of the lasing threshold due to higher absorption coefficient, higher σ_{em}, and higher gain in the anisotropic F8 layer; and (3) a new type of tuning method by the controlling angle between the alignment direction of the aligned F8 and DFB orientation, causing the change in n_{eff}. Finally our method may be attractive for electrically pumped tunable laser device by improved charge transport properties[29] and optically pumped tunable laser device by higher optical gain.

ACKNOWLEDGMENTS

We thank the EPSRC for support. M.H. Song thanks Dr. Y.Y. Noh for technical assistance.

[1] N. Tessler, Adv. Mater. (Weinheim, Ger.) **11**, 363 (1999).
[2] U. Scherf, S. Riechel, U. Lemmer, and R. F. Mahrt, Curr. Opin. Solid State Mater. Sci. **5**, 143 (2001).
[3] G. Heliotis, R. Xia, K. S. Whiehead, G. A. Turnbull, I. D. W. Samuel, and D. D. C. Bradley, Synth. Met. **139**, 727 (2003).
[4] R. Xia, M. Campoy-Quiles, G. Heliotis, P. Stavrinou, K. S. Whiehead, and D. D. C. Bradley, Synth. Met. **155**, 274 (2005).
[5] I. B. Martini, I. M. Craig, W. C. Molenkamp, H. Miyata, S. H. Tolbert, and B. J. Schwartz, Nat. Nanotechnol. **2**, 647 (2007).
[6] H. Lin, C. Lin, C. Wu, T. Chao, and K. Wong, Org. Electron. **8**, 189 (2007).
[7] G. A. Turnbull, P. Andrew, W. L. Barnes, and I. D. W. Samuel, Appl. Phys. Lett. **82**, 313 (2003).
[8] G. Heliotis, R. Xia, G. A. Turbull, P. Andrew, W. L. Barnes, I. D. W. Samuel, and D. D. C. Bradley, Adv. Funct. Mater. **14**, 91 (2004).
[9] R. Xia, G. Heliotis, P. N. Syavrinou, and D. D. C. Bradley, Appl. Phys. Lett. **87**, 031104 (2005).
[10] C. Karnutsch, C. Gýrtner, V. Haug, U. Lemmer, T. Farrell, B. S. Nehls, U. Scherf, J. Wang, T. Weimann, G. Heliotis, C. Pflumm, J. C. deMello, and D. D. C. Bradley, Appl. Phys. Lett. **89**, 201108 (2006).
[11] R. H. Friend, R. W. Gymer, A. B. Holmes, J. H. Burroughes, R. N. Marks, C. Taliani, D. D. C. Bradley, D. A. Dos Santos, J. L. Bredas, M. Logdlund, and W. R. Salaneck, Nature (London) **397**, 121 (1999).
[12] T. Virgili, D. G. Lidzey, M. Grell, D. D. C. Bradley, S. Stagira, M. Zavelani-Rossi, and S. De Silvestri, Appl. Phys. Lett. **80**, 4088 (2002).
[13] T. W. Lee, O. K. Park, H. N. Cho, D. Y. Kim, and Y. C. Kim, J. Appl. Phys. **93**, 1367 (2003).
[14] R. Jakubiak, V. P. Tondiglia, L. V. Natarajan, R. L. Sutherland, P. Lloyd, T. J. Bunning, and R. A. Vaia, Adv. Mater. (Weinheim, Ger.) **17**, 2807 (2005).
[15] J. Zaumseil, R. H. Friend, and H. Sirringhaus, Nat. Mater. **5**, 69 (2006).
[16] M. D. McGehee, M. A. Diaz-Gracia, F. Hide, R. Gupta, E. K. Miler, D. Moses, and A. J. Heeger, Appl. Phys. Lett. **72**, 1536 (1998).
[17] K. Suzuki, K. Takahashi, Y. Seida, K. Shimizu, M. Kumagai, and Y. Taniguchi, Jpn. J. Appl. Phys., Part 2 **42**, L249 (2003).
[18] M. R. Weinberger, G. Langer, A. Pogantsch, A. Haase, E. Zojer, and W. Kern, Adv. Mater. (Weinheim, Ger.) **16**, 130 (2004).
[19] S. Riechel, U. Lemmer, J. Feldman, S. Berleb, A. G. Muckl, W. Brutting, A. Gombert, and V. Wittwer, Opt. Lett. **26**, 593 (2001).
[20] Z. Zheng, K. Yim, M. S. M. Saifullah, M. R. Welland, R. H. Friend, J. Kim, and W. T. S. Huck, Nano Lett. **7**, 987 (2007).
[21] D. R. Barbero, M. S. M. Saifullah, P. Hoffmann, H. J. Mathieu, D. Anderson, G. A. C. Jones, M. E. Welland, and U. Steiner, Adv. Funct. Mater. **17**, 2419 (2007).
[22] J. M. Ziebarth and M. D. McGehee, Appl. Phys. Lett. **83**, 5092 (2003).
[23] D. Wright, E. Brasselet, J. Zyss, G. Langer, and W. Kern, J. Opt. Soc. Am. B **21**, 944 (2004).
[24] M. Pauchard, J. Swensen, D. Moses, A. J. Heeger, E. Perzon, and M. R. Andersson, J. Appl. Phys. **94**, 3543 (2003).
[25] G. F. Barlow, A. Shore, G. A. Turnbull, and I. D. W. Samuel, J. Opt. Soc. Am. B **21**, 2142 (2004).
[26] X. Liu, C. Py, Y. Tao, Y. Li, J. Ding, and M. Day, Appl. Phys. Lett. **84**, 2727 (2004).
[27] W. Holzer, A. Penzkofer, S. Gong, A. Bleyer, and D. D. C. Bradley, Adv. Mater. (Weinheim, Ger.) **8**, 974 (1996).
[28] D. E. McCumber, Phys. Rev. Lett. **136**, A954 (1964).
[29] H. Sirringhaus, R. J. Wilson, R. H. Friend, M. Inbasekaran, W. Wu, E. P. Woo, M. Grell, and D. D. C. Bradley, Appl. Phys. Lett. **77**, 406 (2000).